Eur. Phys. J. D (2022) 76:43
https://doi.org/10.1140/epjd/s10053-022-00371-0

THE EUROPEAN PHYSICAL JOURNAL D

Regular Article – Atomic and Molecular Collisions

R-matrix calculations for elastic electron and positron scattering from pyrazine: effect of the polarization description

Vincent Graves and Jimena D. Gorfinkiel[a]

School of Physical Sciences, The Open University, Walton Hall, Milton Keynes MK7 6AA, UK

Received 26 November 2021 / Accepted 17 February 2022 / Published online 10 March 2022

Abstract. We present R-matrix calculations of electron and positron low energy scattering from the highly polarizable pyrazine molecule. We compare integral and differential elastic cross sections with experimental results and assess the quality of the models used for describing collisions of either projectile. Static-exchange-plus-polarization models give a good description of electron scattering (including that of shape resonances), whereas both the integral and small-angle differential cross sections are underestimated for positron collisions for the same models. We discuss whether the absence of a permanent dipole moment improves the comparison with experiment for this molecule, as well as future calculations that may improve the description of polarization effects and thus positron scattering.

1 Introduction

Low energy electron and positron collisions with molecules take place in a number of natural and man-made environments with the former being, due to the much higher abundance of electrons, significantly more prevalent and therefore the focus of more computational investigations [1]. These works, together with their experimental counterparts, are aimed at providing both quantitative data and fundamental insight into the collisions to help model and control the environments in which they are involved (technological plasmas, radiation used for medical treatment and imaging, etc.). Below the positronium formation threshold, the same approach can be used to model both types of collisions: e.g. the R-matrix [2], Kohn variational [3], Schwinger Multichannel (SMC) [4] methods, single centre approach [5] and convergent close-coupling approach (for H_2) [6]. Their computational implementations can be applied to the study of the low energy interaction of both projectiles with small and medium size molecules. In general, however, these approaches seem to fare better when describing electron scattering, with positrons collision (even below the positronium formation threshold) not always well described.

The lack of exchange interaction between projectile and target electrons in positron scattering could be seen as making the computational modelling of these collisions easier than for electron scattering. This is, however, not the case [2,7,8]. On one hand, since polarization is an attractive interaction for both projectiles, this interaction has the same sign as the (short-range) static interaction in the case of an electron, but opposite sign for a positron; this makes the observables for the latter more sensitive to the polarization description. On the other, the short-range correlation in positron scattering seems to be harder to model than the (anti)correlation of electrons.

As a result, the accurate description of correlation/polarization effects is much more critical in positron calculations. Whereas on the whole, this description no longer seems to pose serious limitations to the modelling of electron scattering, this is not the case for positrons, and this holds true for several of the methods mentioned above. Attempts have been made to improve and modify the approaches: for example, the use of atomic basis functions placed on additional 'dummy' centres in the SMC method [9] or use of a semi-empirical scaling factor to increase the electron–positron attraction integrals in R-matrix calculations [8] that improved their accuracy for a range of molecules [10,11]. Use of pseudostates has also been tried in R-matrix calculations to improve polarization description.

In this paper, we investigate the description of correlation/polarization effects in calculations for positron and electron scattering from the non-polar pyrazine (see Fig. 1) using the R-matrix method. As with all diazines, pyrazine has a polarizability of around 60 a_0^3. With its high polarizability and the dipolar interaction absent, pyrazine is an excellent system to study the effect of polarization description: the low energy behaviour of the cross section will be strongly affected by it and the presence of a Ramsauer–Townsend (RT) minimum and/or a virtual state is possible.

[a] e-mail: J.Gorfinkiel@open.ac.uk (corresponding author)

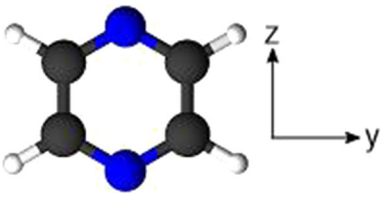

Fig. 1 Pyrazine: blue indicates nitrogen atoms, dark grey carbon and white hydrogen. The coordinate system used in our calculations is indicated on the right

A couple of comprehensive theoretical studies have been performed into electron scattering from pyrazine. Mašín and Gorfinkiel [12] used the R-matrix method to determine elastic and inelastic integral cross sections, elastic differential cross sections and resonance positions. Winstead and McKoy [13,14] also determined elastic cross sections as well as shape resonance energies and widths using the SMC method. Experimental elastic absolute differential and integral cross sections were measured by Palihawadana et al. [15] using a crossed electron-molecular beam spectrometer technique. Resonances in pyrazine were investigated by Nenner and Schulz [16]. The only available publications on positron scattering from pyrazine are a computational study by Moreira and Bettega [17], who used the SMC method to determine the elastic integral and differential cross sections and a recent joint theoretical/experimental work [18] that presents measured elastic, electronic excitation and positronium formation cross sections for scattering energies of 1 to 79 eV as well as cross sections calculated using the R-matrix method (elastic, low energy) and the IAM-SCAR approach (elastic and inelastic, higher energies).

The R-matrix method is described in Sect. 2, emphasizing polarization description. Electron scattering results, based on the work of Mašín and Gorfinkiel [12] are presented in Sect. 4.1 and their agreement with SMC calculations and experiments is discussed. Sect. 4.2 presents our positron calculations and, again, a critical comparison with prior data. Section 4.3 discusses the use of pseudostates to improve the polarization description. Finally, further discussion and conclusions are presented in Sect. 5.

2 The R-matrix method

The R-matrix method has been extensively and successfully applied to the study of electron-molecule scattering below the ionization threshold. A number of publications describe it in detail [2,19]. The calculations in this work have been performed with the UKRmol suite [20] for positrons and the UKRmol+ suite [21] for electrons as the latter was not yet fully tested for positrons. Below, we provide a brief summary of the method and refer the reader to earlier publications for more details. We describe and apply the approach within the fixed-nuclei approximation.

The R-matrix method separates the scattering problem into an inner and an outer region by means of a sphere of radius a. In the inner region, all particles are considered explicitly and exchange and correlation must be taken into account. By contrast, in the outer region the scattering particle becomes distinguishable (in the case of the electron) so exchange can be neglected and the projectile–target interaction is described using a single centre multipole expansion potential. This makes the outer region computationally simpler and cheaper for most calculations. At the boundary of these two regions, the R-matrix is constructed using results from the inner region.

The inner region basis functions $\Psi_k^\Gamma(x_1,...,x_{N+1})$ can be expanded using the Close-Coupling approximation:

$$\begin{aligned}\Psi_k^\Gamma(x_1,...,x_{N+1}) &= \mathcal{A}\sum_{i=1}^{n_b}\sum_{j=1}^{n_{c,i}}\Phi_i(x_1,...,x_N)\gamma_{ij}(x_{N+1})a_{ijk} \\ &\quad+\sum_{i=1}^{m}\chi_i^\Gamma(x_i,...,x_{N+1})b_{ik} \qquad (1)\end{aligned}$$

Here, x_i denotes the four spin and space coordinates of the electron i. The operator $\mathcal{A}$ ensures antisymmetrization of the wavefunctions and is required when the projectile is an electron. The target wavefunctions Φ_i and the L^2 functions χ_i^Γ are built as antisymmetrized products of bound molecular orbitals. The L^2 functions describe the short-range correlation-polarization. The single particle functions γ_{ij} are known as continuum orbitals and describe the projectile. The coefficients a_{ijk} and b_{ik} are determined through the diagonalization of the Hamiltonian matrix in the inner region, made Hermitian by the inclusion of the Bloch operator [2]. n_b is the number of target electronic states included in the calculation and the superscript Γ indicates the irreducible representation of the functions: $\Phi_i(x_1,...,x_N)$ and γ_{ij} must be chosen such that their product has the correct space and spin symmetry.

In this work, the continuum orbitals γ_{ij} are constructed from Gaussian type orbitals (GTOs) centred on the centre of mass of the system. The individual continuum GTOs are first orthogonalized to the target orbitals and then to each other. A deletion threshold is required in the latter orthogonalization step. If this deletion threshold is set too high, too many continuum orbitals are deleted leading to a poor continuum description. Alternatively, if set too low, too many orbitals are kept, which can cause linear dependency issues.

The R-matrix, evaluated at the R-matrix boundary, is used to solve a simpler set of differential questions in the outer region. This is done using a propagation approach [2]. Matching the solutions obtained with their known asymptotic form enables the determination of the scattering energy-dependent K-matrix, that contains all the scattering information produced by the calculations. From the K-matrices, it is trivial to deter-

mine T- and S-matrices and from them integral and differential cross sections. The latter are calculated using POLYDCS [22].

The type and number of L^2 functions, along with the number of target states included, defines the scattering model used. Well defined models regularly employed for electron and positrons scattering are the static (S)/static-exchange (SE) (for positrons and electron, respectively) and Static plus polarization (SP)/static-exchange plus polarization (SEP) models. Both of these include a single target wavefunction in the close-coupling expansion (Eq. 1). When more target state wavefunctions are used, the model is called close-coupling (CC). We briefly explain how polarization is described in these models.

2.1 Description of polarization

Polarization effects are modelled in two ways in R-matrix calculations; (i) by inclusion of the appropriate L^2 functions (at S(E)P and CC levels); (ii) by inclusion of excited states in the CC expansion (CC level). The L^2 configurations used in S(E)P calculations for an N electron target can be schematically written as follows;

$$\mathrm{Core}^{N_c}\ \mathrm{Val}^{N-N_c}\mathrm{VO}^1 \quad \mathrm{Core}^{N_c}\ \mathrm{Val}^{N-N_c-1}\mathrm{VO}^2$$

'Core' indicates a frozen core, containing N_c electrons in doubly occupied orbitals, 'Val' a 'valence' space from which excitations are carried out and VO a set of virtual orbitals, i.e. bound molecular orbitals not included in the target ground state configuration. The VO are occupied by the projectile in the first set of configuration and by the projectile and a target electron in the second set. In addition, when the projectile is a positron, the positron is also allowed to occupy the Core and Val spaces.

In the case of the CC model, it is customary to expand the target wave functions in terms of a complete active space (CAS): $\mathrm{Core}^{N_c}\ \mathrm{CAS}^{N-N_c}$. The L^2 configurations correspond to allowing the projectile to occupy all the orbitals in the active space (again, the positron can also occupy a Core orbital):

$$\mathrm{Core}^{N_c}\mathrm{CAS}^{N-N_c+1}$$

or one of a set of selected VO:

$$\mathrm{Core}^{N_c}\mathrm{CAS}^{N-N_c}\mathrm{VO}^1$$

Note that the Core spaces and N_c in the CC and SEP/SP calculations need not be the same for a given target. Also, for few electron systems, usually N_c=0 and no Core is used. When the polarizability of the molecule is not large, the second set of configurations is not required (this gives a more balanced model [21]).

2.1.1 Pseudostates and pseudocontinuum orbitals

An approach that has been employed to improve (in some cases, converge [23]) the polarization description for small molecules is the inclusion of pseudostates in the calculation. The R-matrix with pseudostates method (RMPS) was first developed to model electron-impact near-threshold ionization [24] and then employed to improve the modelling of positron scattering observables (cross sections, Z-effective) [25,26] as well as electron scattering below the ionization threshold (e.g. [27]).

Pseudostates are eigenfunctions of the molecular Hamiltonian that do not describe true states of the system. In the molecular RMPS approach [21,28] they are built from single excitations from the ground state configuration into a set of pseudocontinuum orbitals (PCOs). These PCOs are, in turn, generated from even tempered GTOs centred on the centre of mass of the system. Their exponents follow a geometrical progression:

$$\alpha_i = \alpha_0\beta^{i-1} \quad i = 1, ..., N \tag{2}$$

with $1 < \beta < 2$. The exponents are the same for different angular momenta l but the number of GTOs used usually decreases as l increases (as is the case for the continuum basis set) up to a specified $l_{\max}^{\mathrm{PCO}}$.

The configurations used to generate the target states and pseudostates can be written as:

$$\mathrm{Core}^{N_c}\mathrm{CAS}^{N-N_c}$$
$$\mathrm{Core}^{N_c}\mathrm{CAS}^{N-N_c-1}\mathrm{PCO}^1$$

and the L^2 functions are thus:

$$\mathrm{Core}^{N_c}\mathrm{CAS}^{N-N_c+1}$$
$$\mathrm{Core}^{N_c}\mathrm{CAS}^{N-N_c}\mathrm{PCO}^1$$

where, once more, the positron can also occupy Core and CAS orbitals (configurations of the type $\mathrm{Core}^{N_c}\ \mathrm{CAS}^{N-N_c-1}\ \mathrm{PCO}^2$ are not usually employed as they make the calculation too big).

As mentioned above, earlier studies seem to show reasonable convergence of the polarizability when pseudostates are included. However, all molecules studied were relatively compact: diatomics, triatomics, or linear molecules like C_2H_2; none had polarizabilities bigger than 25 a_0^3, except Li_2 that has a polarizability over 200 a_0^3.

2.1.2 Evaluation of the polarizability

It isn't possible, in R-matrix studies, to quantify the amount of polarization being described in S(E)P calculations. For CC calculations, one can determine the (implicit) value of the molecular polarizability being modelled in the inner region by the (pseudo)states by calculating it as a sum over said states; for the ground state the expression is:

$$\alpha_{qq} = 2\sum_{n>0} \frac{|\langle \Phi_0|\mu_q|\Phi_n\rangle|^2}{E_n - E_0} \quad (3)$$

where q represents Cartesian components X, Y and Z, n and 0 label an excited and the target ground state, respectively and μ_q is the component of the dipole operator along q. The summation runs over all the states included in the close-coupling expansion. Note that as the energy difference between the excited and ground states increases, the contribution of that state to the polarizability will decrease, leading to convergence. One can use this calculation to estimate how much polarization is being described in a CC calculation.

3 Details of the calculation

Pyrazine belongs to the D_{2h} point group and thus does not possess a permanent dipole moment. However, the molecule does have a large polarizability: an accurately computed (using the DFT method, the B3LYP functional and the 6-311+G(3df,2p) basis set) value for the spherical polarizability [29], along with its diagonal components are listed at the bottom of Table 3 (no experimental data is available). The geometry used in these calculations was taken from an experiment by Innes et al. [30]. The ground state configuration of pyrazine is: $1b_{1u}^2\ 1a_g^2\ 1b_{2u}^2\ 2a_g^2\ 2b_{1u}^2\ 1b_{3g}^2\ 3a_g^2\ 3b_{1u}^2\ 2b_{2u}^2\ 4a_g^2\ 2b_{3g}^2\ 5a_g^2\ 3b_{2u}^2\ 4b_{1u}^2\ 4b_{2u}^2\ 1b_{3u}^2\ 3b_{3g}^2\ 5b_{1u}^2\ 1b_{2g}^2\ 6a_g^2\ 1b_{1g}^2$.

Calculations were performed using a number of models. For the S(E)P calculations, HF orbitals were used to describe the ground state of pyrazine. The CC calculations used CASSCF orbitals determined with MOLPRO: details of the active space and state-averaging can be found in [12]. Five basis sets were tested: two of them, cc-pVDZ and 6-311+G** have been used extensively in previous R-matrix studies of this and similar molecules, so that deletion thresholds for orthogonalization and the required R-matrix radius were known. For the remaining three basis sets, DZP, DZP+diffuse and 6-311++G(3df,3pd) these parameters had to be determined. The most appropriate number of VOs for each calculation was also determined and will be discussed below.

The appropriate R-matrix radius was determined from the orbital amplitudes computed as a function of the distance from the centre of mass using a functionality available in the UKRmol+ suite. The R-matrix radius is chosen to be the smallest possible that ensures the amplitudes of the target orbitals included in the calculation are less than approximately 10^{-4} at the R-matrix boundary. As only GTOs were used for the continuum description, the largest R-matrix radius for which calculations could be sensibly run was 18 a_0. This meant that for the 6-311++G(3df,3pd) basis set some orbitals had to be removed from the calculations as their amplitudes were larger than 10^{-4} even for a=18 a_0. Table 1 summarizes the R-matrix radius and deletion thresholds used for each basis set for which results are presented. The highest continuum partial waves for all calculations was $l = 4$.

Table 1 R-matrix radius, a, and deletion thresholds used for each basis set used in the positrons calculations in this work. Only those thresholds different from 10^{-7} and the orbital symmetry for which they were needed are indicated

Basis Set	a (a_0)	Thresholds
cc-pVDZ	13.00	–
6-311+G**	18.00	10^{-8}: A_g, B_{1g}; 10^{-9}: A_u
6-311++G(3df,3pd)	18.00	10^{-6}: all symmetries
DZP	18.00	–

4 Results

4.1 Electron scattering

Mašín and Gorfinkiel [12] investigated a number of models for electron pyrazine scattering (different basis sets, number of virtual orbitals, active spaces for the CC calculation, etc.) focusing primarily on the description of the resonances. Their best SEP and CC calculations provided a fairly good description of the shape and mixed shape-core excited resonances present: the resonance positions were in reasonable agreement with experiment [16]. Table 2 summarizes the results for the shape resonances.

Figure 2 shows the total elastic cross section calculated at SEP and CC levels using the two basis sets chosen by Mašín and Gorfinkiel for their detailed investigations: cc-pVDZ and 6-311+G**, compared to the SMC [13] and experimental results [15]. It is clear that the CC calculations provide very similar cross sections with small shifts in the π^* resonance positions. The SEP results with the diffuse basis agree reasonably well with Winstead and McKoy's, whereas those using the compact basis set fail to describe the RT minimum (this is more clearly visible in the ^2A_g contributions to the integral elastic cross section, presented in Figs. 3 and 5

Table 2 Energy (in eV) of the 3 lowest energy π^* resonances in pyrazine. R-matrix data calculated at SEP level for the basis sets indicated [12]. Winstead and McKoy's SMC results [13], also at SEP level, were estimated from figures. Experimental results by Nenner and Schulz [16] are shown as resonance centres and ranges of its vibrational broadening (estimated from figures for resonance $^2B_{2g}$)

	$^2B_{3u}$	^2A_u	$^2B_{2g}$
R-matrix, cc-pVDZ	0.44	1.05	5.38
R-matrix, 6-311+G**	0.14	1.12	5.19
Winstead and McKoy	0.15	1.3	4.4
Nenner and Schulz	0.065	0.87	4.10
	0.065–0.8	0.087–1.2	3.8–4.4

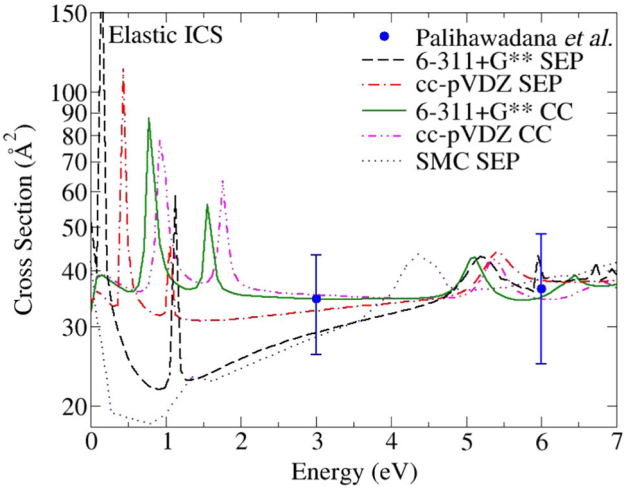

Fig. 2 Integral elastic cross section for electron scattering from pyrazine. Experimental results by Palihawadana *et al.* [15] are shown as blue dots. Computational SMC results by Winstead and McKoy [13] are presented as a purple dotted line. R-matrix calculations computed in this work using the models of Mašín and Gorfinkiel [12] and are shown as dashed and dot-dashed lines with the basis set and method used indicated in the figure

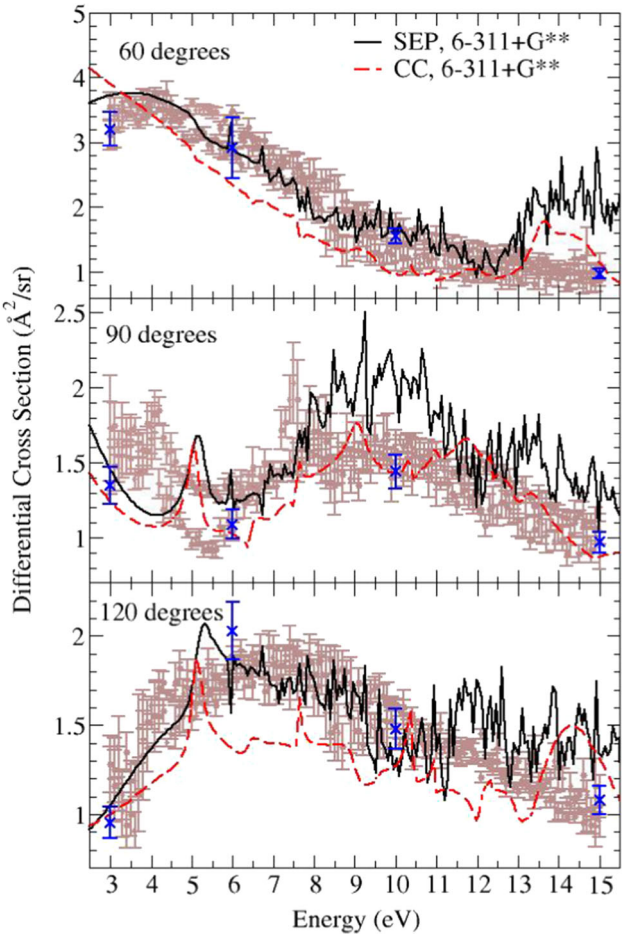

Fig. 3 Elastic excitation functions for electron scattering from pyrazine at 60°, 90° and 120°. Experimental data by Palihawadana et al. [15] are shown as brown data points with angular distribution measurements in blue. The solid and dashed lines are R-matrix calculations computed in this work using the models of Mašín and Gorfinkiel [12]

of [12]). The position of this minimum in the total elastic cross section determined with the best SEP model is a little higher than in SMC calculations [31].

The comparison with experiment in Fig. 2 would lead to the conclusion that it's the CC calculations (and the SEP one with the compact basis set) that provide better agreement with experiment at 3 eV, potentially casting doubt on the presence of the RT minimum, and the conclusion, derived from the resonance positions, that the SEP model with the diffuse basis set provides the best agreement with experiment. However, the quantity actually measured by the experiment is the differential cross section (DCS); below 15 eV the measurements were performed for angles between 30° and 129°, so the integral cross sections in Fig. 2 are the result of extrapolation of these DCS in order to integrate over all angles. A better comparison of experiments and calculation is therefore given by the DCS.

Figure 3 shows excitation functions (DCS for a specific scattering angle as a function of energy). Note that the jagged look of the SEP results is due to the presence of non-physical resonances above ∼6 eV that also lead to the overestimation of the cross section in that energy range. This, together with the fact that inclusion of excited states in the CC calculations usually leads to a somewhat lower elastic cross section than that produced by SEP calculations (and the appearance of physical core-excited resonances), accounts for the noticeable differences between calculated excitation functions; the shift in physical resonances due to different polarization descriptions is clearly visible for 90° and 120°. Nonetheless, we see that the excitation functions calculated at CC and SEP level with the diffuse basis set show similar agreement with those measured by Palihawadana et al., with the SEP results being slightly closer to experiment. Therefore, the difference in the integral cross section at 3 eV must come from the contribution of angles below 60° and/or above 120°.

To investigate this in more detail, Fig. 4 shows the DCS for 3 eV, both for positron and electron scattering. We see clearly here than in the case of electron scattering (the positron one will be discussed in the next section), the experimental DCS at 3 eV agrees quite well with both the SMC results and the R-matrix ones determined at SEP level with the diffuse basis set (the other R-matrix models, not shown, produce DCS that are significantly higher in the angular range 30°-60°). This confirms that, at 3 eV, the higher value of the experimental integral cross section does not come from the measured values of the DCS; the extrapolation of the experimental values below 30° and/or above 130° must overestimate the DCS. This comparison also confirms that the RT minimum is probably physical.

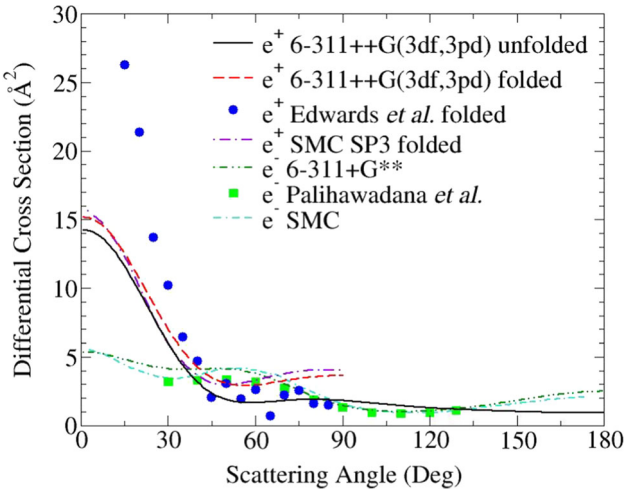

Fig. 4 Elastic differential cross section for electron and positron scattering from pyrazine at 3 eV. Experimental data: blue circles, positron data by Edwards et al. [18] (the measurement at 10° is outside the plotted range); green squares, electron data by Palihawadana et al. [32]. SMC SEP/SP results: purple dot-dashed curve, folded positron data by Moreira and Bettega [17]; cyan dot-dash-dashed curve, electron data by Winstead and McKoy [13]. R-matrix SEP/SP results: green dash-dot-dotted curve, electron scattering; black solid (unfolded) and red dashed (folded) curves, positron data. The basis sets used are indicated in the figure

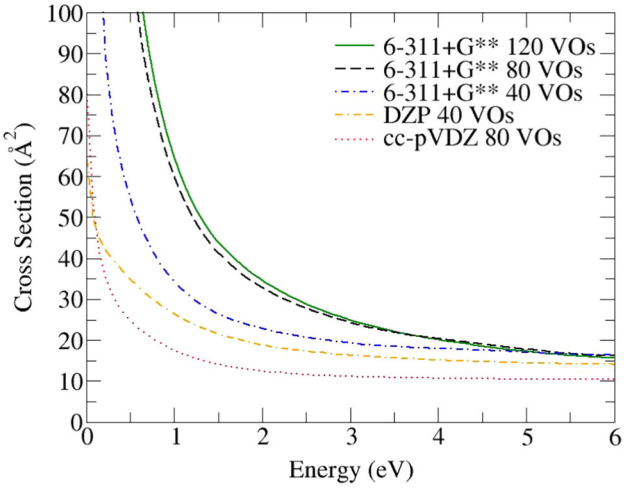

Fig. 5 Integral elastic cross section for positron scattering from pyrazine using an SP model and the basis set and number of VOs indicated in the figure

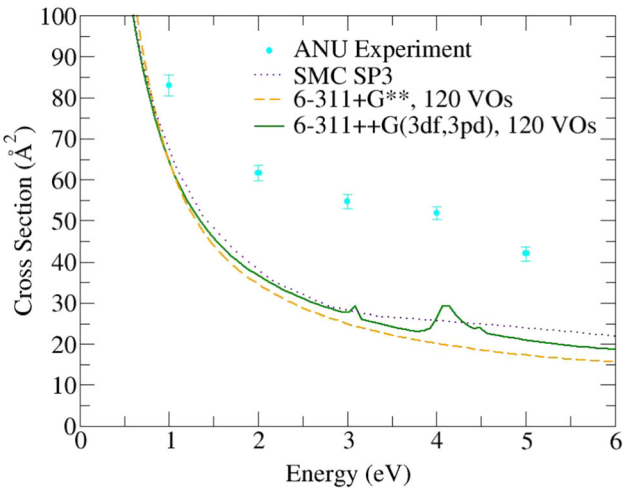

Fig. 6 Integral elastic cross sections for positron scattering from pyrazine using an SP model for the basis set and VOs indicated in the figure. The purple dotted curve corresponds to the SP3 SMC model by Moreira and Bettega [17] and the cyan dots are experimental results from Edwards *et al* [18]

The best model identified for the description of elastic scattering (SEP using a diffuse basis set) describes electron scattering well: the resonance positions, the presence of an RT minimum and the size and shape of the DCS elastic cross sections are well described. It is therefore this model that we expect to provide the best description of positron scattering from pyrazine.

4.2 Positron scattering

Initial positron scattering calculations were based on the SEP models selected by Mašín and Gorfinkiel to study electron scattering from diazines. The SP elastic integral cross sections produced using both the compact and diffuse basis set, as well as the DZP basis, are shown in Fig. 5. One can see that the most diffuse basis set produces the largest cross section for the whole energy range presented and that increasing the number of VOs from that used for electron scattering (40) to 80 has a noticeable effect below 3–4 eV, whereas when increasing them to 120 the effect is significantly smaller.

We also see that the shape of the positron integral cross section is very different to that for electron scattering. The former increases significantly as the energy decreases, so that it is larger than the electron scattering one below ∼3 eV. This increase originates in the ^2A_g symmetry contribution to the cross section and can be attributed to the presence of a virtual state. This behaviour is also observed in the experimental cross section [18] and that calculated by Moreira and Bettega using the SMC method [17], both shown in Fig. 6. Moreira and Bettega determined the scattering length (SL) associated with their results and concluded that it may actually be indicating a bound state, not a virtual state. The quality of the description of this state was dependent on how well the polarizability was described. Our estimates of the scattering length, determined from the A_g eigenphase sum using the same equations provided by Morrison [33] employed by Moreira and Bettega, also point at a bound state, though more weakly bound than that of Moreira and Bettega: we obtain a scattering length of 190–200 a_0 (depending on the energy range fitted) for the calculation using the 6-311+G** basis set and 80 VOs and a value of 68–70 a_0 for the calculation using the 6-311+G** basis set and 120 VOs.

These values correspond to estimated binding energies ($-1/(2*SL^2)$) of 0.34–0.38 meV and 2.8 meV, respectively. Given the approximate nature of these very small binding energies, they should not be taken as definite confirmation of the presence of a bound state.

Figure 5 shows that the choice of target basis set has a significant effect, as was the case for electron scattering: the more compact DPZ and cc-pVDZ calculations produce cross sections that are much smaller than those determined with more diffuse basis sets. This effect is not too different in size to that of increasing VOs from 40 to 80: both influence the quality of the polarization description. This result led us to test the use of an even bigger basis set, 6-311++G(3df,3pd); this result is included in Fig. 6. The cross section shows some non-physical structure at 3 and 4 eV, probably due to linear dependence or small leaking outside the sphere: some of the orbitals included had larger amplitudes at the boundary (7.7×10^{-5}) than for all other calculations. This prevented us from attempting to include more VOs in the calculation. Use of this basis set (and 120 VOs) does not bring the computed value of the cross section much closer to experiment, indicating that something else is required to ensure polarization and correlation effects are sufficiently well described.

We see in Fig. 6 that the R-matrix cross section calculated with the diffuse basis sets agree reasonably well with the SMC result, but that both methods significantly underestimate the experimental cross section. Interestingly, this disagreement is larger at higher energies, rather than at 1 eV where the dependence on the polarization description would be expected to be strongest. The difference for 1 eV is around 20% and close to 50% at 3 eV: for this latter energy the electron scattering cross section was underestimated by the SEP models by less than 30%, and this difference was attributed to the extrapolation used to determine the experimental integral cross sections. For 5 eV, the experimental positron cross section is about twice the calculated one, whereas for electrons, the differences at 6 eV are no bigger than 10%.

Unlike electron scattering, the positron experiment measures DCS and the integral cross section separately. The integral cross section is measured down to an energy-dependent angle: 13.7° at 1 eV decreasing to 4.3° at 10 eV. An energy-dependent 'correction' that corresponds to a percentage of the integrated cross section is employed to account for the missing angles (see [18] for more details). As a result, in the case of positrons it is not possible to make a direct connection between the angular range for which the DCS is measured and the experimental value of the integral cross section. Nonetheless, it is still instructive to compare the measured and calculated DCS. A look at the DCS for 3 eV in Fig. 4 shows that, as is the case for electrons, the SMC and R-matrix SP calculations with the diffuse basis agree reasonably for the whole angular range. The experimental DCS is significantly bigger than the calculated results between the first angle measured (10°) and ∼30° (by almost a factor of 3 at 10°), whereas the calculated DCS are bigger than the experiment between ∼80° and 90°. Note that positron DCS measurements are 'folded' around 90°: the folded DCS for a specific θ correspond to DCS(θ) + DCS(180° - θ). Nonetheless, Fig. 4 shows for 3 eV that the calculated DCS below 30° is around an order of magnitude bigger than above 150°, so that the differences between folded and unfolded DCS is less than 20% for small angles. Around 90°, the DCS is similar in size below and above this angle, so that the folded DCS is around twice the unfolded one.

If one integrates the 3 eV folded experimental and R-matrix DCS *in the angular range for which the DCS is measured*, the experimental cross section is around 12% bigger: a significantly smaller difference than the factor of ∼2 observed in the integral cross section. Interestingly, if one performs the same partial integration for 1 eV, the experimental result is close to 12% *smaller* than the R-matrix one. In this reduced angular range, there is a compensation for positrons between the underestimation of the experimental DCS at small angles (where the sin(θ) is smaller) and its overestimation around 90°. Once again, agreement between experimental and calculated DCS is better than between the integrated cross section: the large differences seen in the integral elastic cross section seem to arise either from the applied correction significantly overestimating the contribution of the missing angular range in the integral cross section measurement or from calculations underestimating the forward-peaked nature of the collisions. Perhaps both. The smaller disagreement at 1 eV may be due to the compensation mentioned earlier.

Figure 7 provides a more detailed comparison of the different models, as it shows the contributions of the different D_{2h} irreducible representations to the integral cross section. The largest contribution below 1 eV is that of the ^2A_g symmetry and it is clearly bigger for the more diffuse basis sets. Above 1 eV this contribution is smaller than 20 Å^2 and the largest contribution is that of the $^2B_{1u}$ followed by the $^2B_{3u}$ symmetry for the diffuse bases but the $^2B_{2u}$ one in the case of the compact basis set. All other contributions are significantly smaller.

The agreement of the symmetry contributions for the diffuse basis sets with those calculated with the SMC approach is, overall, fairly good, although whether the 6-311+G** or the 6-311++G(3df,3pd) one produces better agreement is symmetry dependent. The more noticeable differences can be seen at very low energies, where the energy dependence of the cross section contributions is quite different for symmetries $^2B_{1g}$ and $^2B_{2u}$ (the spike at around 3 eV in this latter symmetry is a non-physical pseudoresonance as is the structure around 4 eV in ^2A_g). The symmetry-by-symmetry agreement shows that the fact that both methods produce integral elastic cross sections of very similar size is not fortuitous. If the discrepancy with experiment is due to limitations in the calculation, these are clearly very similar for the models used in both approaches.

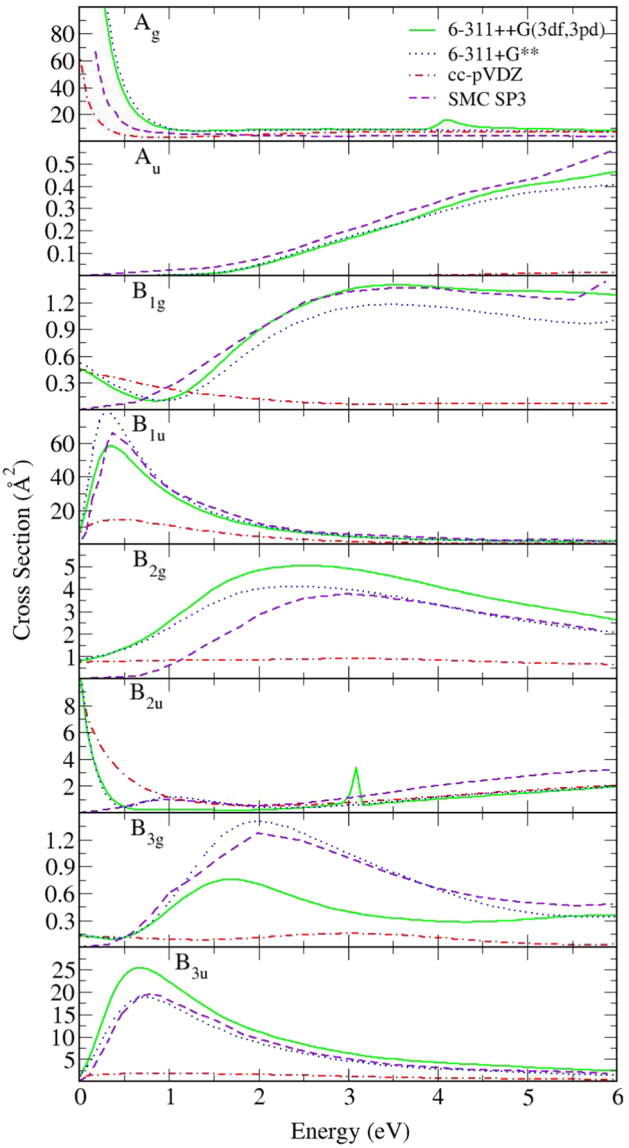

Fig. 7 Symmetry contributions to the integral elastic cross section for positron scattering from pyrazine using SP models. Red dot-dashed curve, cc-pVDZ basis set with 80 VOs; blue dotted curve, 6-311+G** basis set with 120 VOs and green solid curve, 6-311++G(3df,3pd) basis set using 120 VOs. Purple dashed curve, SP3 SMC model by Moreira and Bettega [17]

4.3 Testing PCO use

Inclusion of pseudostates in the calculation can improve the modelling of polarization effects so we investigated the effect of using of PCOs on the target polarization description: different $l_{\max}^{\mathrm{PCO}}$ and number of pseudostates were used for the calculation of the polarizability using Eq. 3. The parameters to generate the PCO exponents (Eq. 2) and deletion thresholds (used in the orthogonalization of these orbitals) were chosen, following previous studies [25,34], to be $\alpha_0 = 0.17$, $\beta = 1.4$ and 2×10^{-4}, respectively. HF target orbitals were used for these tests.

Table 3 summarizes the results. Even the largest calculations including PCOs and pseudostates (models 1 and 8) produce a spherical polarizability of 36–37 a_0^3, less than 65% of the calculated accurate value of around 59 a_0^3. One can also see that the effect of using a different target basis set is not large: about 1% for $l_{\max}^{\mathrm{PCO}}$=5 and 400 pseudostates, and around 10% for $l_{\max}^{\mathrm{PCO}}$=4 and 200 pseudostates

The results also seem to show that increasing $l_{\max}^{\mathrm{PCO}}$ has a small effect if the number of pseudostates included in the calculation remains the same (compare, for example, models 2 and 3). However, increasing the number of states for a specific $l_{\max}^{\mathrm{PCO}}$, does have a significant effect on the value of the polarizability (see, in this case, models 1 and 2). Model 9 shows the effect of using a different number of PCOs for different partial waves: here 8 PCOs are used for $l \leq 3$ and 4 PCOs for $l > 3$. The spherical polarizability is almost identical to the one obtained when 8 PCOs are used for all l (model 8). This may point at a way of reducing the size of the integral calculation without a noticeable reduction in size of the polarization even for bigger models.

We note that from the practical point of view, increasing $l_{\max}^{\mathrm{PCO}}$ implies a bigger integral calculation, while increasing the number of pseudostates increases the size of Hamiltonian to diagonalize and can also lead to the inclusion of more channels in the outer region. Nonetheless, it is clear from Table 3 that using more pseudostates leads to a better description of the polarization but that the best values obtained are still around 30% smaller than accurate results

Given the unsatisfactory description of the polarizability of pyrazine when PCOs are used, we performed an additional type of test. This involves generating the same type of configurations as those used in the above calculations, but using VOs instead of PCOs. The configurations generated are no different to those used in standard SEP/SP calculations; the difference is that in this case these configurations are used to describe pseudostates in addition to being included as L^2 ones. We call this model Close-coupling Hartree–Fock (it is related to the Polarization Consistent Coupled Hartree-Fock, PCCHF, used in R-matrix photoionization calculations [35]), to indicate that the (pseudo)states included in the CC expansion are all described in terms of a single configuration/Slater determinant. It is clear from the results at the bottom of Table 3, generated using 80 VOs, that this produces significantly better values for the polarizabilities than the use of PCOs: use of 400 states produces a polarizability almost identical to the accurate value. Even use of 200 states gives a polarizability of around 44 a_0^3, better than that obtained for the same target basis set and 400 states when PCOs are used (model 1). This model leads to a smaller calculation, both because fewer integrals need to be computed as no pseudocontinuum basis is included, and because fewer target states provide a better description of the polarizability. Electron scattering calculations with this model and 40 VOs showed a small low-

Table 3 Effect of various parameters related to the use of PCOs on the calculations of the polarizability of pyrazine

#	Basis Set	Number of States	l_{max}^{PCO}	Number of PCOs	Spherical	Polarizability Components			Number of CSF
					Polarizability	XX	YY	ZZ	
1	6-311+G**	400	5	288	36.78	22.88	46.44	41.02	772
2	6-311+G**	200	5	288	28.34	14.27	40.03	30.70	772
3	6-311+G**	200	4	200	25.75	16.18	31.72	29.36	570
4	6-311+G**	100	4	200	19.33	13.93	23.95	20.11	570
5	6-311+G**	100	3	128	19.25	14.45	23.32	19.99	404
6	6-311+G**	10	3	128	12.51	1.249	18.75	17.54	404
7	6-311+G**	10	3	64	12.75	1.206	19.20	17.83	315
8	6-311+G**	10	5	288	10.92	1.110	16.38	15.26	772
9	6-311+G**	10	5	208	10.60	0.000	16.47	15.32	614
10	cc-pVDZ	400	5	288	36.41	22.51	46.01	40.71	772
11	cc-pVDZ	200	4	200	25.69	15.46	32.59	29.03	570
CC-HF	6-311+G**	80	–	–	29.41	12.72	41.18	34.32	150
CC-HF	6-311+G**	200	–	–	44.07	20.02	62.11	49.89	150
CC-HF	6-311+G**	400	–	–	58.43	32.54	75.27	63.47	–
Accurate value		–	–	–	58.62	36.71	74.46	64.69	–

For the models identified with a number, the total number of PCOs is obtained as $8\sum_{l_{\max}^{\mathrm{PCO}}}(2l_{\max}^{\mathrm{PCO}}+1)$ (except for model 9 that used 8 PCOs for $l \leq 3$ and 4 PCOs for $l > 3$). The models labelled CC-HF did not use PCOs (see text for details). The number of CSFs is averaged over all irreducible representations. The accurate value is from the CCCBDB and was calculated using the DFT method B3LYP and 6-311+G(3df,2p) basis set [29]. The spherical polarizability and its components are given in a_0^2. The *X*-, *Y*- and *Z*-axes correspond to those indicated in Fig. 1

ering of the π^* resonances (around 0.25 eV) that turned the $^2B_{3u}$ into a bound state; it also leads to changes at very low energies in the A_g contribution that might indicate the presence of a virtual state. We think it likely that both these states (the bound and virtual) are not physical and that this model is overcorrelated for electron scattering. Unfortunately, attempts to perform positron calculations using these CC-HF models lead to significant linear dependence. Use of a B-spline basis set for the continuum [21] may alleviate this problem.

5 Discussion and conclusions

We have performed R-matrix calculations for electron and positrons scattering from pyrazine and compared our integral and differential elastic cross sections with experiment and SMC calculations in order to assess how well polarization and correlation effects are described.

In the case of electron scattering, we have confirmed that discrepancies at low energies (3 eV) in the integral cross section are mainly due to the extrapolations required to generate the experimental integral value. Both experiment and theory produce a significantly more forward peaked DCS for positron than electrons. However, the calculated positron DCS does not increase as much as the angle decreases. It is unlikely the calculations are underestimating the backward scattering DCS by a factor close to 10, so it seems to be the modelling of the small angle (forward) scattering that, although qualitatively correct, it is quantitatively inconsistent with experiment for positrons. It is perhaps this underestimation of the forward-angle contribution to the calculated integral cross section (particularity for the very small angles, for which there are no measurements) that is a significant contributor to the disagreement of the positron integral cross sections.

Both for positron and electron scattering the SMC and R-matrix SEP/SP calculations produce integral elastic cross sections in very good agreement. We conclude that the models used in both calculations are of a similar quality: this is sufficient to capture the main effects influencing the collision for electron scattering, but this is not the case for positron as a projectile. Whether the issue is related to the description of polarization effects or correlation/anticorrelation is not possible to say as these can't be separated in our calculations.

When choosing pyrazine for these studies, an assumption was made that, due to the lack of dipolar interaction, the comparison with experiment would be more straightforward and therefore better than for a similar, but polar, target. The reason is that, for polar molecules, use of a Born-based top-up is necessary to fully account for the projectile–permanent dipole interaction [2] and model the behaviours of the DCS, that is very forward peaked, and the integral cross section, that grows rapidly as the energy tends to 0 eV. This top-up is understood to be less accurate than the *ab initio* calculations. In this respect, a comparison with results for pyrimidine, an isomer of pyrazine with a significant dipole moment, can shed some light.

The R-matrix method has been applied to the study of electron and positron scattering from pyrimidine. For electron scattering, elastic DCS agree very well with experiment for the measured angular range, except for very low energies (i.e. 1 eV) [36]; the Born-corrected integral cross section overestimated experiment, but the agreement was very good if the integral cross section was determined integrating the uncorrected DCS with their behaviour between 0° and 2° modified (see details in [36]). The corrected and uncorrected DCS are virtually identical for angles above a certain value (30° for 3 eV decreasing to 10° for 10 eV). So the better agreement when uncorrected DCS were used (with some modifications) seemed to indicate that the Born correction overestimates the forward scattering cross sections.

For pyrazine, it is the experiment that overestimates the integral cross section at low energies. For this target, the inaccuracy of the (unnecessary) Born correction cannot be the source of the discrepancy. The agreement between R-matrix results and experiment seems, overall, of a similar quality for both targets.

Positron scattering from pyrimidine has also been studied with the R-matrix method [37]: comparison with experiment [38] was analysed by Barbosa et al. [39] who also presented SMC results. The comparison at angles around 90° is similar to that for pyrazine: the calculations overestimate the experimental DCS. At smaller angles, however, agreement is better: the experimental cross section is larger than the calculated ones, but the forward-peaked nature of the Born-corrected DCS means they are closer to the experimental values. As a result, the calculated integral elastic cross section is larger than the experimental one, the R-matrix one (calculated as SP level with a diffuse basis set) more so than the SMC and with the disagreement increasing as the scattering energy decreases. In this case, therefore, it seems that R-matrix method (and the SMC) describe the collisions with the dipolar target better than for pyrazine.

It is interesting to note that the models used for the electron-pyrimidine calculations mentioned above produce both accurate electronic excitation cross sections (to bands of states) and core-excited resonances: both agreed very well with high-quality experiments [40]. The position of the latter however, was shifted to higher energies in the calculations: this was interpreted to be the result of an insufficient description of the polarization effects.

Calculations of the polarizability of pyrazine using the sum-over-states expression and including a number of pseudostates and PCOs show that, at least for the PCOs and number of pseudostates tested, the approach does not significantly improve the value of the polarizability. A better approach for this seems to be to include in the CC expansion more target states built as single excitations from the ground state configuration to virtual orbitals (CC-HF model). This may prove a route to improving the polarization description and, perhaps agreement with experiments. Future work will focus on running these type of calculations, as well as standard CC ones, with the UKRmol+ suite, where use of B-splines for the continuum description should eliminate linear dependence problems; the suite is also computationally much more efficient making it easier to run bigger calculations with many more target states.

Acknowledgements V. G. acknowledges support from the EPSRC Doctoral Training Partnership EP/T518165/1. We acknowledge support from the Australian Research Council Discovery program (DP190100696). We are also grateful to Dr. Zdeněk Mašín who performed detailed work on the study of electron scattering from diazines and Dr. James Sullivan who motivated the choice of pyrazine for this study.

Author contributions

V.G. performed all new calculations presented in this paper. V.G. and J.D.G. contributed equally to the writing of the manuscript.

Data Availability Statement This manuscript has associated data in a data repository. [Authors' comment: The data corresponding to the calculations presented in this publication is available here: https://doi.org/10.21954/ou.rd.17099063.v1.]

References

1. S. Schippers, E. Sokell, F. Aumayr, H. Sadeghpour, K. Ueda, I. Bray, K. Bartschat, A. Murray, J. Tennyson, A. Dorn et al., J. Phys. B Atomic Mol. Optic. Phys. **52**, 171002 (2019)
2. J. Tennyson, Phys. Rep. **491**, 29 (2010)
3. C.W. McCurdy, T.N. Rescigno, Phys. Rev. A **39**, 4487 (1989)
4. R.F. da Costa, M. T. do N. Varella, M.H.F. Bettega, M.A.P. Lima, Eur. Phys. Journal D **69**, 159 (2015)
5. N. Sanna, G. Morelli, S. Orlandini, I. Baccarelli, Comput. Phys. Commun. **235**, 366 (2019)
6. M.C. Zammit, D.V. Fursa, J.S. Savage, I. Bray, J. Phys. B Atomic Mol. Optic. Phys. **50**, 123001 (2017)

7. C.M. Surko, G.F. Gribakin, S.J. Buckman, J. Phys. B **38**, R57 (2005)
8. J. Franz, K. Baluja, R. Zhang, J. Tennyson, Nuclear Instruments and Methods in Physics Research Section B: Beam Interactions with Materials and Atoms **266**, 419 (2008), low Energy Positron and Positronium Physics
9. A.S. Barbosa, S. d'A. Sanchez, M.H.F. Bettega, Phys. Rev. A **96**, 062706 (2017)
10. J. Franz, F.A. Gianturco, K.L. Baluja, J. Tennyson, R. Carey, R. Montuoro, R.R. Lucchese, T. Stoecklin, P. Nicholas, T.L. Gibson, Nucl. Instrum. Methods Phys. Res., Sect. B **266**, 425 (2008)
11. J. Franz, M. Franz, Eur. Phys. J. D **73**, 1 (2019)
12. Z. Mašín, J.D. Gorfinkiel, J. Chem. Phys. **135**(14144 14), 144308 (2011)
13. C. Winstead, V. McKoy, Phys. Rev. A **76**, 012712 (2007)
14. C. Winstead, V. McKoy, Phys. Rev. Lett. **98**, 113201 (2007)
15. P. Palihawadana, J.P. Sullivan, S.J. Buckman, M.J. Brunger, J. Chem. Phys. **137**, 204307 (2012)
16. I. Nenner, G.J. Schulz, J. Chem. Phys. **62**, 1747 (1975)
17. G.M. Moreira, M.H.F. Bettega, J. Phys. Chem. A **123**, 9132 (2019)
18. D. Edwards, D. Stevens, Z. Cheong, V. Graves, J.D. Gorfinkiel, F. Blanco, G. Garcia, M.J. Brunger, R.D. White, J.P. Sullivan, Phys. Rev. A **104**, 042807 (2021)
19. P.G. Burke, *R-Matrix Theory of Atomic Collisions: Application to Atomic, Molecular and Optical Processes* (Springer, Berlin, 2011)
20. J.M. Carr, P.G. Galiatsatos, J.D. Gorfinkiel, A.G. Harvey, M.A. Lysaght, D. Madden, Z. Mašín, M. Plummer, J. Tennyson, H.N. Varambhia, Eur. Phys. J. D **66** (2012)
21. Z. Mašín, J. Benda, J.D. Gorfinkiel, A.G. Harvey, J. Tennyson, Comput. Phys. Commun. **249**, 107092 (2020)
22. N. Sanna, F. Gianturco, Comput. Phys. Commun. **114**, 142 (1998)
23. M. Jones, J. Tennyson, J. Phys. B Atomic Mol. Optic. Phys. **43**, 041501 (2010)
24. J.D. Gorfinkiel, J. Tennyson, J. Phys. B Atomic Mol. Optic. Phys. **38**, 1607 (2005)
25. R. Zhang, P.G. Galiatsatos, J. Tennyson, J. Phys. B Atomic Mol. Optic. Phys. **44**, 195203 (2011)
26. K.L. Baluja, R. Zhang, J. Franz, J. Tennyson, J. Phys. B Atomic Mol. Opt. Phys. **40**, 3515 (2007)
27. M. Tarana, J. Tennyson, J. Phys. B Atomic Mol. Opt. Phys. **41**, 205204 (2008)
28. J.D. Gorfinkiel, J. Tennyson, J. Phys. B Atomic Mol. Optic. Phys. **37**, L343 (2004)
29. R.D. Johnson, *Computational Chemistry Comparison and Benchmark Database, NIST Standard Reference Database 101* (2019)
30. K.K. Innes, I.G. Ross, W.R. Moomaw, J. Mol. Spectrosc. **132**, 492 (1988)
31. H.P. Pritchard, V. McKoy, M.A.P. Lima, Phys. Rev. A **41**, 546 (1990)
32. P. Palihawadana, J. Sullivan, M. Brunger, C. Winstead, V. McKoy, G. García, F. Blanco, S. Buckman, Phys. Rev. A **84**, 062702 (2011)
33. M.A. Morrison, Phys. Rev. A **25**, 1445 (1982)
34. R. Zhang, Ph.D. thesis, University College London (2020)
35. T. Meltzer, Z. Mašín, J. Phys. B **55**, 035201 (2022). https://doi.org/10.1088/1361-6455/ac4d74
36. K. Regeta, M. Allan, C. Winstead, V. McKoy, Z. Mašín, J.D. Gorfinkiel, J. Chem. Phys. **144**, 024301 (2016)
37. A.G. Sanz, M.C. Fuss, F. Blanco, Z. Mašín, J.D. Gorfinkiel, R.P. McEachran, M.J. Brunger, G. García, Phys. Rev. A **88**, 062704 (2013)
38. P. Palihawadana, R. Boadle, L. Chiari, E.K. Anderson, J.R. Machacek, M.J. Brunger, S.J. Buckman, J.P. Sullivan, Phys. Rev. A **88**, 012717 (2013)
39. A.S. Barbosa, D.F. Pastega, M.H.F. Bettega, J. Chem. Phys. **143**, 244316 (2015)
40. K. Regeta, M. Allan, Z. Mašín, J.D. Gorfinkiel, J. Chem. Phys. **144**, 024302 (2016)